ANALYSIS OF GALVANIC COUPLING IN FASTENER/PLATE CONFIGURATIONS

Rebecca Skelton Marshall, Robert G. Kelly

University of Virginia

Abstract

In a realistic aerospace structure, dissimilar metals are used for different components to optimize the final mechanical properties of the assembly. In the presence of an electrolyte, such as rain or condensation, current can flow between the dissimilar metals which induces corrosion via the galvanic couple. In this work specifically, galvanic coupling between AA7075, SS316, and Ti-6Al-4V in a complex fastener-in-panel geometry was studied using finite element modeling (FEM). The model was first validated through comparisons of predictions to experimental results both conducted in-house and from literature. Following validation, the model was extended to predict the severity and location of peak damage. A parameter space was explored that included the effects of both environmental and external variations. It was determined that external surface defects (such as a scratch) and thin water layer thicknesses are important parameters in locating where the peak corrosion will occur. The worst-case scenario found in this work represents thin water layers (44.5 μm) and small defects, which concentrate the corrosion damage inside of the fastener hole, the most highly loaded area. Conversely, the best-case scenario tested represents thicker water layers (>800 μm) and large surface defects.

Introduction

In many aircraft structures, galvanic couples are unavoidably formed between fasteners made of noble materials (e.g., stainless steel, titanium) and the main load-carrying structure made of aluminum alloys (e.g., AA7075-T651)[1,2]. The galvanic couple accelerates the corrosion damage rate of the aluminum alloy, which can create challenges to maintaining the structural integrity of the aircraft. The overarching goal of this research was to understand and predict the galvanic coupling produced by SS316, Ti-6Al-4V, and AA7075-T651 from a modeling and experimental perspective.

Finite element models have been used in literature to determine the current distributions of galvanic couples on both simple and complex geometries, as FEM provides a robust framework for solving complex problems[3–6] When dealing with an aircraft, the complex geometry of important structures increases the difficulty in modeling the galvanic couple. An occluded cell can be formed by the hole wall of the plate and the bolt of the fastener within the hole which can trap aggressive species and further accelerate corrosion damage. The majority of the literature has focused on either corrosion occurring on the surface of the panel[2,7–9], or on corrosion within the fastener hole[10–12]. This work aims to understand both areas of corrosion, and how they may be impacted by each other.

Methods

To monitor corrosion in the geometry described above, this research used an accelerated galvanic corrosion test plate designed by Matzdorf *et al.*[2]. Referred to in this research as the “test panel”, it consists of cathodic fasteners and hardware assembled in a coated aluminum plate. Scribes were placed on the surface of the coated aluminum plate in an “X” pattern to simulate defects in the coating and to allow a pathway for water to travel into the fastener hole.

Test panels were exposed to 504 hours of ASTM B117[13], in which the constant spray of aggressive species (5 wt% NaCl) acts as an accelerant to corrosion. Samples were then removed from the salt spray chamber, and the coating, fasteners, and washers were stripped off. To quantify the corrosion damage inside of each fastener hole, cross-sections were taken by a precision cut-off saw and samples were polished down to 3 μm. Optical profilometry was used to image the polished samples. Further experimental methodology can be found in Marshall *et al.*[14].

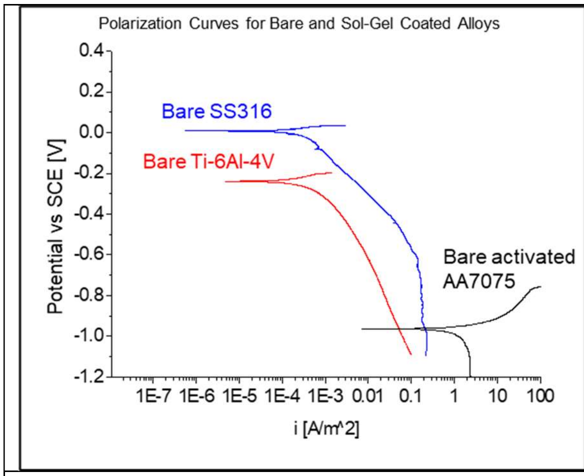

Figure 1: Cathodic and anodic potentiodynamic scans in 5 wt% NaCl on bare SS316, bare Ti-6Al-4V, and bare activated AA7075

A finite element model was built in COMSOL Multiphysics® to simulate the experimental panel, using the same alloys and geometry as described above. All fasteners were assumed to be dry-installed, *i.e.* no sealant inside of the fastener holes, representing a worst-case albeit sometimes realistic scenario[2]. The surface of the AA7075 panel was assumed to be perfect, with zero flux across all boundaries except the prescribed "X" scribes. Simulations to date were run using steady-state conditions, assuming the corrosion is currently taking place and active in the system.

The model in this work used experimentally-derived potentiodynamic scans as boundary conditions, to accurately represent the surface reactions occurring. To best replicate the test panel's exposure to ASTM B117, cathodic and anodic potentiodynamic scans were conducted in 5 wt% NaCl (Figure 1). The water layer thickness during the continuous salt spray of B117 has recently been investigated and determined to be very dependent on the angle of exposure[15]. This work chose a water layer thickness of 4,000 μm to be used when replicating B117, as it has been shown to best match experimental results for corroded surfaces.

Although a simplification of the processes taking place, the Laplace equation ($\nabla^2\Phi = 0$) was chosen as the governing equation. This equation assumes that the migration of ions is the dominant mass transport method, as opposed to diffusion or convection, and is believed to be valid for our system. Furthermore, the conductivity in the electrolyte domain was assumed to be constant, which commonly occurs in the presence of a supporting electrolyte such as NaCl in our scenario. Further details of the model and experimental panel can be found in Marshall *et al.*[14,16].

Results and Discussion

Model Validation

After removal from the testing chamber, the surfaces of AA7075 panels were qualitatively compared with the predicted panel surface from the model (Figure 2). It is important to note that the experimental panel is showing mass loss due to corrosion (Figure 2[a]) while the model visualizes a false-color plot of current density (Figure 2 [b]). Mass loss and current density are directly proportional via Faraday's Law of Electrolysis and can therefore be directly compared. One significant finding from this comparison was that the predicted peak current density (denoted by dark red) at the tips of the scribes was seen experimentally at the bottom right fastener (SS316).

To quantify the experimental results, an in-house MATLAB code extracted statistical corrosion damage from the cross-sectional micrographs of the fastener holes[17]. Results of mass-loss were converted to charge via Faraday's Law of Electrolysis for alloys. Note that this conversion required an assumption that the corrosion damage seen in the cross-section represented the damage throughout the entire fastener hole. The data from two cross-sections of each fastener hole were averaged to give a better estimation of the total damage within the fastener hole and are included as error bars (Figure 2[c]).

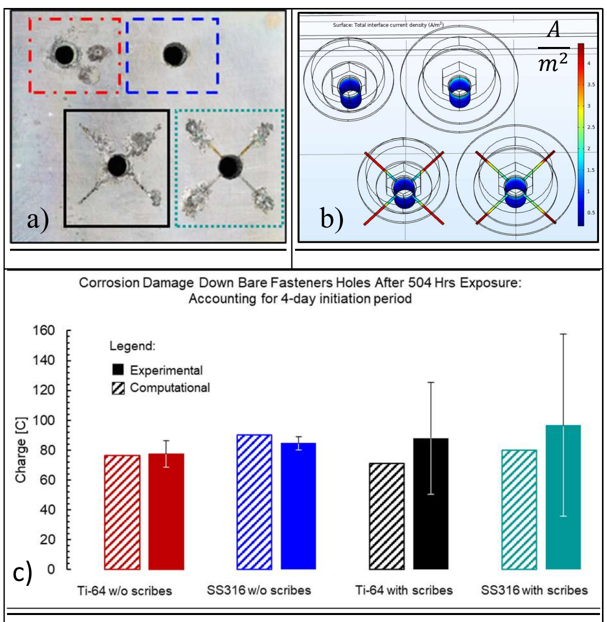

Figure 2: (a) AA7075 plate after 504 hours of exposure to ASTM B117 with coatings and hardware stripped off; (b) false-color current density plot of exposed AA7075 plate under 4,000 μm water layer thickness; (c) comparison of computational (striped bars) vs. experimental data (solid bars) of charge within fastener holes after 504 hours of exposure to ASTM B117. Note the colored boxes in (a) correlate to the results in each fastener hole in (c)[14]

Within the model, the current density was integrated over the anodic fastener hole surfaces to calculate the current. The current was multiplied by the experimental exposure time to determine the total anodic *charge* within the fastener holes which could be directly compared with the experimentally determined charge calculated above. A slight caveat to the conversion between current and charge, is that the current model is calculating *steady-state* corrosion and cannot account for the amount of time required for *corrosion initiation.* Therefore, a four-day initiation period seen from literature was utilized when converting current to charge[7,18,19] to account for the delay in the onset of corrosion.

Results for each fastener hole are seen in Figure 2[c]. It can be seen that despite simplifying assumptions, the model calculated results very similar to those obtained experimentally. Note also that the damage within the fastener holes was relatively constant, regardless of the fastener/washer material type. This was found to be due to the SS316 hardware interacting with all 4 fastener holes, despite their 1 inch separation distance[14].

The qualitative and quantitative comparisons above serve as a reference point for the remaining work, confirming that the model can predict both the severity and distribution of corrosion in this system.

<u>Investigation of External and Environmental Parameters Impacting Galvanic Corrosion</u>

A modified geometry was created in the finite element model to simulate one fastener in a panel, with scribes surrounding the fastener hole in an "X" pattern. This modification was done to eliminate the impact of interactions between the fasteners as was demonstrated to occur in the test panel[14]. Both the scribes and inside of the fastener hole were considered "active structural material" while the fastener and washer were deemed "active fastener";

the remaining boundaries were assumed to have a perfect coating and therefore had no flux at the boundary, as assumed previously. The panel was subjected to a 4,000 μm thick layer of 5% NaCl solution, in a steady-state model, again replicating the scenario of ASTM B117. The current density was calculated at one scribe tip, as a function of expanding scribe length, to determine the interaction distance between a SS316 fastener and washer when coupled with exposed AA7075. This interaction distance can be thought of as a "throwing power" or distance at which the cathodic material can galvanically couple with the anodic material.

It was found that with increasing scribe length, the current density decayed to the self-dissolution rate of the AA7075 panel (Figure 3). This decay indicated that at large scribe lengths, the SS316 fastener was no longer significantly galvanically coupling with the farthest part of the AA7075 panel. Rather, at the tips of long scribes, the panel was corroding at a rate equal to that of a panel containing zero fasteners. As the interaction distance increased, the ohmic resistance in the solution also increased, until the driving force to corrode AA7075 was no longer the fastener but was the reduction reaction of the AA7075 itself.

At scribe lengths of 30 inches, the SS316 hardware did not make a significant contribution to the dissolution current of the AA7075, although the contribution was non-zero. At scribe lengths of approximately 2 inches, the SS316 caused dissolution at *double* the self-corrosion current density of AA7075. The significance of this finding is that coating defects 2 inches away from fasteners are in danger of accelerated corrosion via galvanic coupling. This assessment also helps understand the phenomenon seen experimentally, where the SS316 fastener was coupling with the bare AA7075 fastener hole one inch away[14]. This finding indicates that the dimensions of a surface defect (scribe) can have a large impact on the location of corrosion damage.

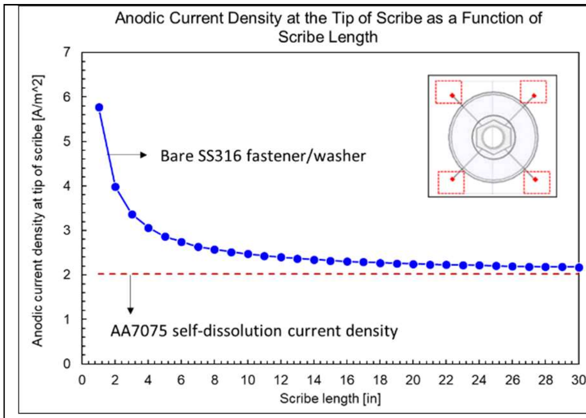

Figure 3: AA7075 anodic current density at the scribe tip vs. scribe length, decaying to the self-dissolution current of AA7075. Inset image serves as a reminder that the plotted current is only from the *tip* of the scribe, and not the total anodic current density[16]

The water layer thickness in the one-fastener configuration was varied both above and below the natural convection boundary layer thickness, which has been determined in literature to be 800 μm within the given environment[20,21]. At water layers greater than 800 μm, there was negligible changes to the system. However, at water layers below 800 μm, both the magnitude and distribution of current density were dramatically impacted, alluding to the fact that thin water layer thicknesses also play an important role in predicting corrosion. An increase in current density magnitude with decreasing water layer thicknesses is consistent with the one-dimensional limiting current density equation below,

$$i_{lim} = \left(\frac{nFD_{O_2,bulk}\left(C_{O_2,bulk}-C_{O_2,surface}\right)}{\delta}\right) \qquad (1)$$

Where n is the number of moles, i_{lim} is the limiting current density, F is Faraday's constant, D is the diffusivity of oxygen, C is

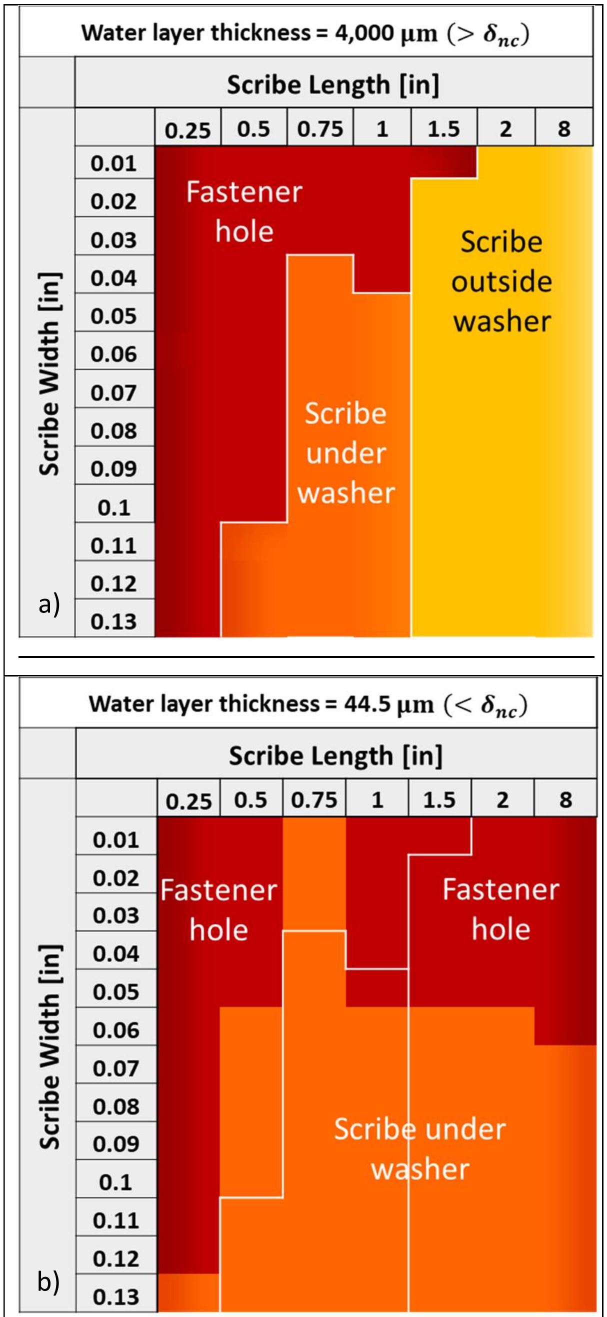

Figure 5: Damage distribution "maps" denoting the majority of the current in the parameter space of scribe dimension and water layer thickness; (a) at a water layer thickness of 4,000 μm, where the white lines represent boundaries between the different locations of interest; (b) at a water layer thickness of 44.5 μm, where the white lines represent the boundaries in (a). Note that δ_{nc} refers to the natural convection boundary layer thickness

the concentration, and δ is the water layer thickness value below the natural convection boundary layer thickness[20].

Peak Damage Distribution "Maps"

Through the analysis above, the dimensions of a surface defect and water layer thickness in a fastener/panel design were both determined to impact the galvanic corrosion. Therefore, to further study the distribution of corrosion damage an investigation in this parameter space was conducted.

The scribes' length and width were varied, to simulate a range of surface defects that could easily occur in a realistic application. The water layer thickness range again spanned across the natural convection threshold, with more focus on extremely thin water layers. The current distribution was deconvoluted into three distinct areas of the anodic surfaces: the fastener hole, the portion of the scribe underneath the washer, and the portion of the scribe outside of the washer (Figure 4).

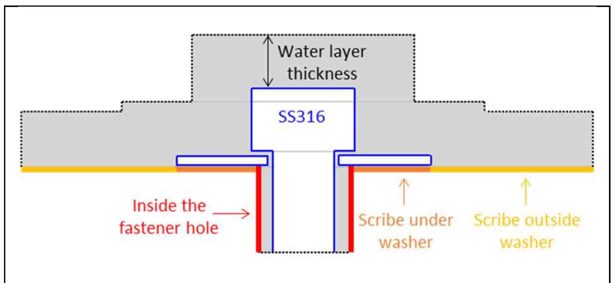

Figure 4: Schematic showing deconvoluted AA7075 surfaces, as represented by the red, orange, and yellow lines. Blue surfaces represent SS316 boundaries, and the grey domain represents the water layer thickness.

The location at which the *greatest* current occurred was documented for each parameter set explored. Plotting these locations on a false-color "map" allows for quick visualization of which scenarios are more favorable than others (Figure 5).

The worst-case scenario occurs when the majority of the corrosion is within the fastener hole (dark red), as this location is a known stress-concentrator[22]. Corrosion damage within this location can further accelerate crack nucleation[23,24]. Conversely, if corrosion was unavoidable, the least damaging location for it to occur would be in the scribes outside of the washer (yellow). This location allows for easy corrosion detection, is not a specific stress-concentrator, and can be spread out over a large area. Corrosion concentrated in the portion of the scribe underneath the washer (orange) is neither the worst nor best condition, because the region is occluded and difficult to detect, but is not a stress-concentrating region.

This damage distribution map can be thought of as a "stop-light" map, as scenarios in red represent the worst-case and call for a hard "stop" while scenarios represented in yellow merit caution but are the most favorable in the given conditions.

When bulk water layer conditions were tested, the majority of the current fell in all three regions of interest, depending on the scribe dimensions (Figure 5[a]). Counterintuitively, *large* scribe lengths are more favorable to small scribe lengths, because the corrosion can be spread out on the surface rather than concentrating inside of the fastener hole. The scribe width had little effect on the outcome of the damage distribution in this water layer thickness.

As the water layer thickness was decreased nearly two orders of magnitude, the distribution of the peak damage changed dramatically. First, the majority of damage no longer occurred in the scribe outside of the washer, regardless of the scribe's dimension (Figure 5[b]). The orange and red locations have also increased in the parameter space, as the white boundary lines from Figure 5[a] are no longer accurate. Another interesting observation is that the scribe width has become a more important parameter than the scribe length, in describing the damage distribution. All of the results above indicate that thin water layers offer a very unfavorable scenario, as opposed to bulk water layer thicknesses.

Conclusion

Investigating corrosion on and around fastener holes has many lasting implications for aerospace structures. For further versatility, using FEM allowed a framework to be developed in which alloys and boundary conditions could be easily modified and catered to every unique situation. Therefore, this research is intended not only to save money and inform the public about the hazards of corrosion, but also to increase the safety of current and further aircraft design. This aligns with NASA's mission, to aim for constant improvement of safety and efficiency.

Specifically, in this work, a finite element model was created with simplifying assumptions and was verified through experimental analysis. This model was then utilized to investigate two parameters of interest, the dimensions of a surface defect and the water layer thickness, and their effect on corrosion damage distribution. Variations to the scribe length showed that a SS316 fastener and washer can still create a significant galvanic couple with bare AA7075 more than 2 inches away. An investigation of the water layer thickness revealed that the natural convection boundary layer thickness is an important threshold. Water layer thicknesses smaller than this threshold resulted in dramatic changes to the galvanic current magnitude and distribution, whereas water layer thicknesses larger than this threshold had negligible impact on the current.

Combining the two parameters of interest (scribe dimension and water layer thickness), a damage "map" was constructed to inform best- and worst-case scenarios for real applications. It was determined that a best-case scenario, to limit corrosion inside of the fastener hole, would include a large water layer thickness and large surface defect. Conversely, small water layer thicknesses and small surface defects should be avoided.

Acknowledgements

Any opinions, findings and conclusions or recommendations expressed in this material are those of the author(s) and do not necessarily reflect the views of Office of Naval Research. This work is supported by the Office of Naval Research under Contract No. N68335-16-C-0121 (Mr. William Nickerson) through a subcontract with Luna Innovations, Inc.

Furthermore, discussions with colleagues at the Center for Electrochemical Science and Engineering (CESE), specifically Katherine Define, at the University of Virginia are greatly acknowledged.

References

1. Aluminum 7075-T6; 7075-T651. *ASM Aerospace Specification Metals Inc* Available at: http://asm.matweb.com/search/SpecificMaterial.asp?bassnum=ma7075t6. (Accessed: 11th June 2018)
2. Matzdorf, C. A. *et al.* Galvanic test panels for accelerated corrosion testing of coated al alloys: Part 1 - Concept. *Corrosion* **69**, 1240–1246 (2013).
3. Liu, C., Kubacki, G. W. & Kelly, R. G. Application of Laplace Equation-Based Modeling into Corrosion Damage Prediction for Galvanic Coupling Between a Zinc Plate and Stainless Steel Rods Under a Thin Film Electrolyte. *Corros. J.* **75**, 465–473 (2019).
4. Turner, M. & Gutierrez-miravete, E. Modeling Galvanic Corrosion. in *COMSOL Conference* 1–4 (2013).
5. Adey, R., Peratta, A., Baynham, J. & Curtin, T. Predicting Cumulative Galvanic Corrosion Damage in Aircraft Structures. in *North Atlantic Treaty Organization Science and Technology Organization* 1–14 (2018).
6. King, A. D., Lee, J. S. & Scully, J. R. Finite Element Analysis of the Galvanic Couple Current and Potential Distribution between Mg and 2024-T351 in a Mg Rich Primer Configuration. *J. Electrochem. Soc.* 342–356 (2016).
7. Feng, Z., Frankel, G. S. & Matzdorf, C. A. Quantification of Accelerated Corrosion Testing of Coated AA7075-T6. *J. Electrochem. Soc.* **161**, 42–49 (2014).
8. Feng, Z., Frankel, G. S., Abbott, W. H. & Matzdorf, C. A. Galvanic attack of coated al alloy panels in laboratory and field exposure. *Corrosion* **72**, 342–355 (2016).
9. Feng, Z. & Frankel, G. S. Galvanic test panels for accelerated corrosion testing of coated al alloys: Part 2 - Measurement of galvanic interaction. *Corrosion* **70**, 95–106 (2014).
10. Liu, C., Rafla, V. N., Scully, J. R. & Kelly, R. G. Mathematical modeling of potential and current distributions for atmospheric corrosion of galvanic coupling in airframe components. *NACE Int. Corros.* (2015).
11. Young, P. S. & Payer, J. H. Stages of Damage Evolution for Al 2024-T3 Around Fasteners in Marine Atmosphere. *CORROSION* **71**, 1278–1293 (2015).
12. Moran, A. *et al.* Coating Breakdown

and Galvanically Accelerated Crevice Corrosion of Aluminum Alloys 2024 and 7075 at Cadmium-Plated Steel Fasteners. *Corros. J.* **75**, 484–498 (2019).

13. *ASTM B117. Standard Practice for Operating Salt Spray (Fog) Apparatus* (ASTM International, 1994).

14. Marshall, R. S., Kelly, R., Goff, A. & Sprinkle, C. Galvanic Corrosion Between Coated Al Alloy Plate and Stainless Steel Fasteners, Part 1: FEM Model Development and Validation. *Corrosion* **75**, 1461–1473 (2019).

15. Katona, R. M., Tokuda, S., Perry, J. & Kelly, R. G. Design, construction, and validation for in-situ water layer thickness determination during accelerated corrosion testing. *Corros. Sci.* **175**, 108849 (2020).

16. Marshall, R. S., Goff, A., Sprinkle, C., Britos, A. & Kelly, R. Estimating the Throwing Power of SS316 When Coupled with AA7075 Through Finite Element Modeling. *Corrosion* **76**, 476–484 (2020).

17. Tattersall, C. Modeling and Analysis of Geometrically Complex Corrosion. (University of Virginia, 2018).

18. Feng, Z., Boerstler, J., Frankel, G. S. & Matzdorf, C. A. Effect of surface pretreatment on galvanic attack of coated Al alloy panels. *Corrosion* **71**, 771–783 (2015).

19. Boerstler, J. T. Corrosion Degradation of Coated Aluminum Alloy Systems through Galvanic Interactions. (The Ohio State University, 2018).

20. Liu, C., Srinivasan, J. & Kelly, R. G. Editors' Choice — Electrolyte Film Thickness Effects on the Cathodic Current Availability in a Galvanic Couple. *J. Electrochem. Soc.* **164**, C845–C855 (2017).

21. Katona, R. *et al.* Editors' Choice — Natural Convection Boundary Layer Thickness at Elevated Chloride Concentrations and Temperatures and the Effects on a Galvanic Couple. *J. Electrochem. Soc.* **168**, (2021).

22. Mcmurtrey, M. D., Bae, D. & Burns, J. T. Fracture mechanics modelling of constant and variable amplitude fatigue behaviour of fi eld corroded 7075-T6511 aluminium. (2016). doi:10.1111/ffe.12536

23. Burns, J. T., Larsen, J. M. & Gangloff, R. P. Effect of initiation feature on microstructure-scale fatigue crack propagation in Al-Zn-Mg-Cu. *Int. J. Fatigue* **42**, 104–121 (2012).

24. Burns, J. T., Larsen, J. M. & Gangloff, R. P. Driving forces for localized corrosion-to-fatigue crack transition in Al–Zn–Mg–Cu. *Fatigue Fract. Eng. Mater. Struct.* **34**, 745–773 (2011).